PERGAMON

PII: S1359-6454(98)00427-3

Acta mater. Vol. 47, No. 4, pp. 1379–1388, 1999

Printed in Great Britain
1359-6454/99 $19.00 + 0.00

A NUMERICAL MODEL OF PERITECTIC TRANSFORMATION

A. DAS, I. MANNA and S. K. PABI

Department of Metallurgical and Materials Engineering, Indian Institute of Technology, Kharagpur 721302, India

(Received 17 April 1998; accepted 1 October 1998)

Abstract—A rigorous numerical model of peritectic transformation kinetics based on the solution of unsteady state diffusion equations in moving phase fields has been presented. The overall and interface mass balance equations are solved to calculate the rate of movement of the interfaces. The predictions of the present formulation show a better agreement with the experimental kinetic data from the Cd–Ag and Pb–Bi systems, compared to those of the earlier proposed models based on quasi-static interface or quasi-steady state approximations. It is predicted that the presence of coring in the primary solid (β) would not have any appreciable effect on the kinetics of peritectic transformation, especially, prior to the consumption of the liquid phase unless the product phase (α) has a restricted composition range. Furthermore, the kinetics remain practically unaltered irrespective of a linear or cored initial concentration gradient in the α-phase. However, the assumption of a linear concentration gradient in α throughout the course of the transformation may significantly underestimate the kinetics. © *1999 Acta Metallurgica Inc. Published by Elsevier Science Ltd. All rights reserved.*

1. INTRODUCTION

Peritectic change may be described as [1]: liquid + primary/reactant solid (β) $\rightarrow$ secondary/product solid (α). The phase change occurring during cooling through the peritectic isotherm involves three different stages [2]. The first stage (i.e. peritectic reaction) is governed by solute diffusion through the liquid when α forms and quickly envelopes the primary β-particles. As a consequence, the reactant phases lose contact with each other. Subsequently, the second stage (i.e. peritectic transformation) proceeds by solute diffusion through the α-layer. Besides the peritectic transformation, the remnant liquid may often directly solidify into α in the third stage. The second or peritectic transformation stage is the slowest step involved in this phase change that seldom reaches completion, and thus, results in microsegregation [3]. Peritectic change has so far been utilized mainly for grain refinement in some Al-based alloys [4–7], liquid route processing of YBCO superconductors [8–13] and development of magnetic materials [14–17]. Though peritectic change is a common invariant reaction in the metallic/ceramic systems, a comprehensive understanding of its mechanism and kinetics is still lacking. An extremely slow reaction kinetics and the presence of liquid in the microstructure pose difficulties in experimental investigations. Moreover, a microstructural distinction between the α formed through peritectic transformation and through direct solidification of the remnant liquid often becomes too difficult. As an alternative, mathematical modelling has been attempted in the past to elucidate the kinetics of different stages of the peritectic change, especially, the peritectic transformation. From the results of solid–liquid diffusion couple experiments, Titchner and Spittle [18] concluded that a power relationship of the type $w = At^n$ is valid for the thickening of α-rim (w) as a function of time (t), where A is related to the different equilibrium concentration terms and n is the time exponent varying from 0.35 to 0.57 depending on the alloy system chosen. Similar expressions have been derived by St. John and Hogan [19] utilizing the Wagner expression [20] for intermediate phase growth to describe w as a function of t in the form: $w = B\sqrt{2t}$ where B is another function of the concentration values.

Maxwell and Hellawell [6] have used Laplacian approximation to represent the solute distribution profiles in α and liquid phases, and solved mass balance equations to calculate the rate of displacement of the concerned interfaces assuming nearly invariant α–β interface position. However, it may be noted that the Maxwell and Hellawell model is restricted only to dilute alloys and, if a prior diffusion layer in the liquid is assumed to exist, peritectic transformation seems to be analogous to α-crystallization from the melt.

In a more rigorous analytical treatment, Lopez [21] attempted to consider a cored concentration profile in the β-phase for the first time while predicting the peritectic transformation kinetics.

The Lopez model considers quasi-static interface locations and a time-invariant profile in the β-phase. However, it has previously been demonstrated that the quasi-static interface approximation may significantly overestimate the kinetics of precipitate dissolution [22] and, hence it is essential to examine whether this is an appropriate assumption for predicting the peritectic transformation kinetics.

In a recent formulation, Das *et al.* [23, 24] have applied the linearized gradient approximation of Zener [25] to formulate an analytical model and demonstrated that this assumption is better suited than the quasi-static interface or Laplacian approximation. However, the former model neglects the effects of initial concentration gradient in the solid phases on the kinetics. It may be pointed out that an analytical solution is severely restricted by the assumption of specific concentration gradients in the different phases. Thus, a numerical solution is essential to consider the effect of time modulation of concentration profiles in the finite diffusion fields with moving boundaries.

Chuang *et al.* [3] have attempted numerical solutions of peritectic transformation in steel by combining the unsteady state diffusion equation with material balance across the β–α and α–liquid interfaces. Although the solution was worked out for continuous cooling, it did not take into account the effect of freezing rate. Furthermore, the pro-peritectic phase was assumed to be homogeneous in this calculation.

Another model for peritectic transformation in low alloy steels was proposed by Fredriksson [26] assuming dilute alloy behavior and considering a complete equilibrium distribution of carbon. However, the formulation neglected the time modulation of concentration profiles and the effects of impingement of the diffusion fields in the course of the transformation. Fredriksson and Nylén [27] also formulated a more general numerical solution for peritectic transformation assuming a homogeneous β and liquid, and a linear concentration gradient in the α-phase.

It appears that most of the models presented earlier employ several simplifying assumptions to solve the peritectic kinetics, which may not be realistic. Moreover, the solids are assumed to be homogeneous in the majority of cases and the effect of pre-existing concentration gradients in the solids has been ignored. Therefore, a more rigorous numerical treatment for peritectic transformation kinetics is presented that takes into account the effects of unsteady state diffusion in finite diffusion fields and the coring in the solids. The results predicted by the present model have been compared with the experimental kinetic data from the Cd–Ag and Pb–Bi systems, as well as, predictions from the models proposed earlier.

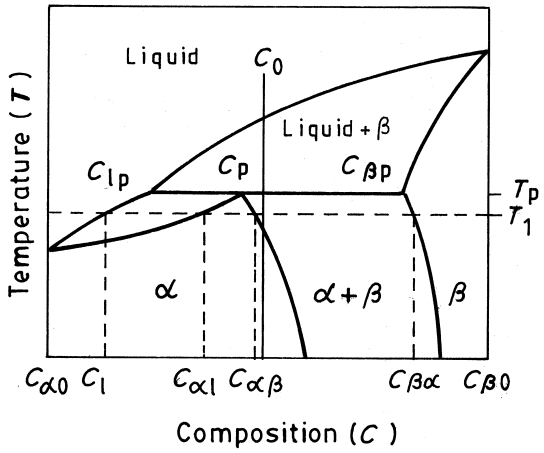

Fig. 1. A schematic binary peritectic phase diagram defining the concentration terms used in the model.

2. THE NUMERICAL MODEL

2.1. Formulation of the problem

Consider the schematic binary phase diagram in Fig. 1 illustrating a typical peritectic change below the peritectic isotherm at T_p. For uniformly sized and equispaced β-particles, the overall kinetics may be represented by the transformation in an isolated and spherically symmetrical cell of radius $R_i = (3/4N_\beta)^{1/3}$, where N_β is the number of β nuclei per unit volume [Fig. 2(a)]. Concentration–distance

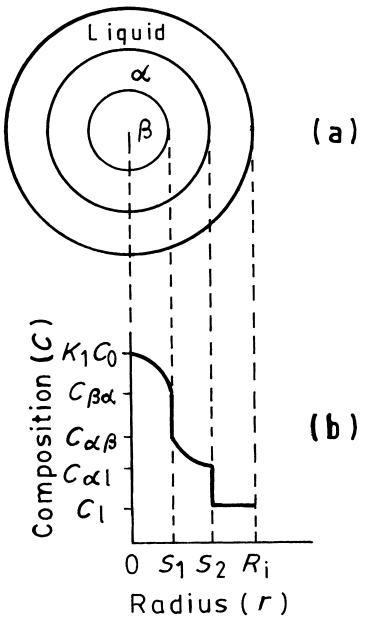

Fig. 2. (a) Schematic representation of the idealized peritectic transformation cell and, (b) the concentration–distance profiles in it during isothermal transformation in an alloy of composition C_0 of Fig. 1 at T_1. K_1 is the equilibrium solute distribution coefficient between β and liquid.

profiles in the respective phases at an isothermal transformation temperature, T_1 ($< T_p$) are represented in Fig. 2(b).

The concentration profile inside the β-phase formed on cooling a liquid of composition C_0 to the peritectic temperature (T_p) may be described by Scheil's equation as

$$C_\beta = K_1 C_0[1 - (r/R_i)^3]^{K_1 - 1} \tag{1}$$

where K_1 is the equilibrium solute distribution coefficient between β and liquid, and r is the spatial variable. Therefore, the β-phase radius (S_{1p}) at the onset of the reaction at T_p may be obtained from

$$S_{1p} = R_i[1 - (C_{\beta p}/K_1 C_0)^{1/(K_1 - 1)}]^{1/3}. \tag{2}$$

On further cooling to the transformation temperature T_1 ($< T_p$), α is assumed to form through solidification of liquid of concentration C_{lp} at T_p. This assumption is in agreement with St. John's [28] observation that α more likely forms through solidification rather than the peritectic reaction for most peritectic systems. Again, a normal segregation profile is expected to exist in α, so that the composition in α may be represented as

$$C_\alpha = K_2 C_{lp}[1 - (r^3 - S_{1p}^3)/(R_i^3 - S_{1p}^3)]^{K_2 - 1} \tag{3}$$

where K_2 is the equilibrium solute distribution coefficient between α and liquid. The outer radius of α (S_{2p}), when α fully envelopes β, i.e. at the outset of the transformation may then be calculated as

$$S_{2p} = [S_{1p}^3 + \{R_i^3 - S_{1p}^3\} \times \{1 - (C_{\alpha l}/K_2 C_{lp})^{1/(K_2 - 1)}\}]^{1/3}. \tag{4}$$

It may be noted that S_{1p} and S_{2p} are the locations of the respective moving interfaces S_1 and S_2 at transformation time $t = 0$.

For a diffusion controlled transformation the respective concentrations in the β- and α-phases at the β–α interface (S_1) at T_1 are given by $C_{\beta\alpha}$ and $C_{\alpha\beta}$ (Fig. 1). Similarly, the concentrations of α and liquid at the α–liquid interface (S_2) at T_1 are given by $C_{\alpha l}$ and C_l, respectively. Furthermore, mass transfer rate in the liquid phase is considered to be much faster than either of the solid phases to make the liquid phase homogeneous with composition C_l during the isothermal transformation at T_1.

Concentration profiles in the solid phases during the course of the transformation ($t > 0$) are given by the field equations

$$\frac{\partial C_\beta}{\partial t} = \frac{1}{r^2}\frac{\partial}{\partial r}\left(r^2 D_\beta \frac{\partial C_\beta}{\partial r}\right) \tag{5}$$

and

$$\frac{\partial C_\alpha}{\partial t} = \frac{1}{r^2}\frac{\partial}{\partial r}\left(r^2 D_\alpha \frac{\partial C_\alpha}{\partial r}\right) \tag{6}$$

where D_β and D_α are the interdiffusion coefficients in β and α, respectively. The β–α interface position is expressed through the interface mass balance equation

$$(C_{\beta\alpha} - C_{\alpha\beta})\frac{dS_1}{dt} = -D_\beta\left(\frac{\partial C_\beta}{\partial r}\right)_{r=S_1} + D_\alpha\left(\frac{\partial C_\alpha}{\partial r}\right)_{r=S_1}. \tag{7}$$

On the other hand, the α–liquid interface location is solved through the following overall mass balance equation:

$$4\pi\int_0^{S_1} C_\beta r^2\,dr + 4\pi\int_{S_1}^{S_2} C_\alpha r^2\,dr + 4\pi\int_{S_2}^{R_i} C_l r^2\,dr = 4\pi\int_0^{R_i} C_0 r^2\,dr. \tag{8}$$

An exact analytical solution of the coupled equations (5)–(8) is not feasible. However, they may be solved numerically to yield the solute distribution in β and α, and the location of the respective interfaces as a function of t.

2.2. Numerical analysis

A direct finite difference representation of equations (5)–(8) is difficult because the thickness of each phase changes throughout the course of the transformation. Tanzilli and Heckel [29] have earlier used the variable grid space transformation (VGST) of Murray and Landis [30] to overcome a similar moving boundary problem in the case of precipitate dissolution. In the present analysis, such VGST is adopted to transform the differential equations.

The rate of change of concentration (C_n) at a point (n) at a radial distance r_n from the center of the transformation cell may be represented as

$$\frac{dC_n}{dt} = \frac{\partial C_n}{\partial r_n}\left(\frac{dr_n}{dt}\right) + \frac{\partial C_n}{\partial t}. \tag{9}$$

Combining equation (9) with the general form of the diffusion field equation

$$\frac{\partial C}{\partial t} = \frac{1}{r^2}\frac{\partial}{\partial r}\left(r^2 D\frac{\partial C}{\partial r}\right)$$

it is found that

$$\frac{dC_n}{dt} = \frac{\partial C_n}{\partial r_n}\left(\frac{dr_n}{dt}\right) + D\left[\frac{\partial^2 C_n}{\partial r_n^2} + \frac{2}{r_n}\frac{\partial C_n}{\partial r_n}\right] \tag{10}$$

where the interdiffusion coefficient D is taken to be independent of composition. The finite difference nomenclature for the spherical cell in Fig. 2 is described in Fig. 3. The nth grid point in the β-phase is defined as $r_n = MS_1$, where M is a constant. Accordingly, equation (10) is rewritten for the β-phase as follows:

$$\frac{dC_n^\beta}{dt} = \frac{r_n}{S_1}\frac{\partial C_n}{\partial r_n}\frac{dS_1}{dt} + D_\beta\left[\frac{\partial^2 C_n}{\partial r_n^2} + \frac{2}{r_n}\frac{\partial C_n}{\partial r_n}\right]. \tag{11}$$

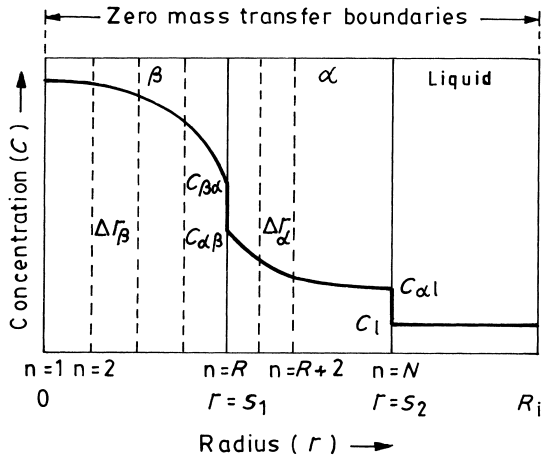

Fig. 3. Schematic concentration–distance profiles illustrating the finite difference nomenclature adopted for the spherical cell in Fig. 2.

In the α-phase the nth grid point may be expressed as $r_n = S_1 + M'[S_2 - S_1]$, where M' is another constant. Therefore, the field equation (10) takes the following form for the α-phase:

$$\frac{dC_n^\alpha}{dt} = \frac{\partial C_n}{\partial r_n}\left[\frac{dS_1}{dt} + \frac{r_n - S_1}{S_2 - S_1}\left(\frac{dS_2}{dt} - \frac{dS_1}{dt}\right)\right] + D_\alpha\left[\frac{\partial^2 C_n}{\partial r_n^2} + \frac{2}{r_n}\frac{\partial C_n}{\partial r_n}\right]. \quad (12)$$

2.3. Finite difference scheme

Rewriting equation (11) in the finite difference form leads to the following expression for the β-phase:

$$\frac{C_n^{i+1} - C_n^i}{\Delta t} = \frac{(n-1)}{S_1^i}\frac{(C_{n+1}^i - C_{n-1}^i)}{2}\frac{(S_1^{i+1} - S_1^i)}{\Delta t} + D_\beta(R-1)^2\frac{(C_{n-1}^i - 2C_n^i + C_{n+1}^i)}{(S_1^i)^2} + D_\beta(R-1)^2\frac{(C_{n+1}^i - C_{n-1}^i)}{(n-1)(S_1^i)^2}. \quad (13)$$

However, the concentration at the first grid point located at the center of the β-phase may be approximated as [31]

$$\frac{C_1^{i+1} - C_1^i}{\Delta t} = 6D_\beta(R-1)^2\frac{(C_2^i - C_1^i)}{(S_1^i)^2} \quad (14)$$

since the corresponding concentration profile is symmetric about this point. For the α-phase, the finite difference representation of the diffusion field equation (12) is given by

$$\frac{C_n^{i+1} - C_n^i}{\Delta t} = \frac{N-R}{S_2^i - S_1^i}\frac{(C_{n+1}^i - C_{n-1}^i)}{2} \times \left[\frac{(S_1^{i+1} - S_1^i)}{\Delta t} + \frac{n-R}{N-R} \times \left(\frac{S_2^{i+1} - S_2^i}{\Delta t} - \frac{S_1^{i+1} - S_1^i}{\Delta t}\right)\right] + D_\alpha\left(\frac{N-R}{S_2^i - S_1^i}\right)^2(C_{n-1}^i - 2C_n^i + C_{n+1}^i) + D_\alpha\left(\frac{N-R}{S_2^i - S_1^i}\right)\frac{(C_{n+1}^i - C_{n-1}^i)}{\left[S_1^i + \frac{n-R}{N-R}(S_2^i - S_1^i)\right]}. \quad (15)$$

2.3.1. Location of the α–β interface. The α–β interface mass balance equation (7) transforms to the following finite difference equation:

$$\frac{S_1^{i+1} - S_1^i}{\Delta t} = \frac{1}{(C_{\beta\alpha} - C_{\alpha\beta})}\left[D_\alpha\left(\frac{N-R}{S_2^i - S_1^i}\right) \times \left(\frac{-C_{R+2}^i + 4C_{R+1}^i - 3C_{\alpha\beta}}{2}\right) - D_\beta\left(\frac{R-1}{S_1^i}\right) \times \left(\frac{C_{R-2}^i - 4C_{R-1}^i + 3C_{\beta\alpha}}{2}\right)\right]. \quad (16)$$

2.3.2. Location of α–liquid interface. At a given instance, the α–liquid interface position can be found by solving equation (8). The total solute content in the transformation cell of radius R_i is given by

$$4\pi\int_0^{R_i} C_0 r^2\,dr = \frac{4\pi}{3}C_0 R_i^3. \quad (17)$$

Similarly, the amount of solute in the liquid at a given t at T_1 may be calculated as

$$4\pi\int_{S_2}^{R_i} C_l r^2\,dr = \frac{4\pi}{3}C_l(R_i^3 - S_2^3). \quad (18)$$

Total solute content in the β-phase may be evaluated numerically using Simpson's formula [32] as

$$4\pi\int_0^{S_1} C_\beta r^2\,dr = \frac{4\pi}{3}\left(\frac{S_1^{i+1}}{R-1}\right)^3\left[(R-1)^2 C_{\beta\alpha} + 2\sum_{n=3,5,\ldots}^{R-2}(n-1)^2 C_n^{i+1} + 4\sum_{n=2,4,\ldots}^{R-1}(n-1)^2 C_n^{i+1}\right] \quad (19)$$

if $(R-1)$ is even (cf. Fig. 3). Similarly, the net

amount of solute present in the α-phase can be estimated from the following expression:

$$4\pi\int_{S_1}^{S_2} C_\alpha r^2\,\mathrm{d}r = \frac{4\pi}{3}(S_1^{i+1})^2\left(\frac{S_2^{i+1}-S_1^{i+1}}{N-R}\right)\times\left[C_{\alpha\beta}+C_{\alpha 1}+2\sum_{n=R+2,R+4,\ldots}^{N-2}C_n^{i+1}+4\times\sum_{n=R+1,R+3,\ldots}^{N-1}C_n^{i+1}\right]+\frac{4\pi}{3}\left(\frac{S_2^{i+1}-S_1^{i+1}}{N-R}\right)^3\left[(N-R)^2C_{\alpha 1}+2\times\sum_{n=R+2,R+4,\ldots}^{N-2}(n-R)^2C_n^{i+1}+4\sum_{n=R+1,R+3,\ldots}^{N-1}\times(n-R)^2C_n^{i+1}\right]+\frac{8\pi}{3}(S_1^{i+1})\times\left(\frac{S_2^{i+1}-S_1^{i+1}}{N-R}\right)^2\left[(N-R)C_{\alpha 1}+2\times\sum_{n=R+2,R+4,\ldots}^{N-2}(n-R)C_n^{i+1}+4\times\sum_{n=R+1,R+3,\ldots}^{N-1}(n-R)C_n^{i+1}\right]. \quad (20)$$

The following equation is obtained by substituting equations (17)–(20) in equation (8) and rearranging:

$$(S_2^{i+1}-S_1^{i+1})^3A-(S_2^{i+1})^3C_1+(S_2^{i+1}-S_1^{i+1})\times(S_1^{i+1})^2B+(S_2^{i+1}-S_1^{i+1})^2(S_1^{i+1})E+(S_1^{i+1})^3F=0 \quad (21)$$

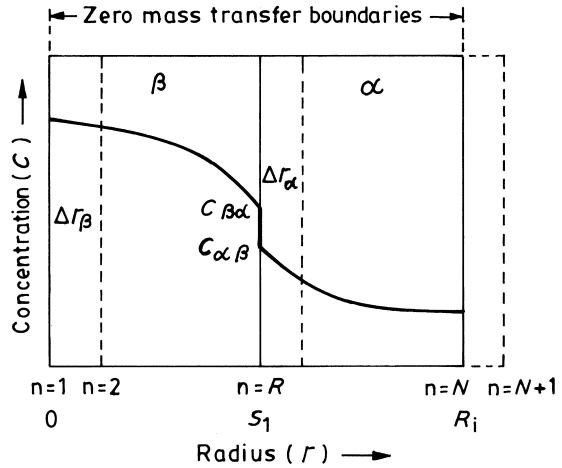

Fig. 4. Modified representation of the finite difference nomenclature presented in Fig. 3 following the consumption of liquid.

where

$$A=\frac{1}{(N-R)^3}\left[(N-R)^2C_{\alpha 1}+2\sum_{n=R+2,R+4,\ldots}^{N-2}(n-R)^2C_{\alpha n}^{i+1}+4\sum_{n=R+1,R+3,\ldots}^{N-1}(n-R)^2C_{\alpha n}^{i+1}\right],$$

$$B=\frac{1}{N-R}\left[C_{\alpha\beta}+C_{\alpha 1}+2\sum_{n=R+2,R+4,\ldots}^{N-2}C_{\alpha n}^{i+1}+4\sum_{n=R+1,R+3,\ldots}^{N-1}C_{\alpha n}^{i+1}\right],$$

$$E=\frac{2}{(N-R)^2}\left[(N-R)C_{\alpha 1}+2\sum_{n=R+2,R+4,\ldots}^{N-2}(n-R)C_{\alpha n}^{i+1}+4\sum_{n=R+1,R+3,\ldots}^{N-1}(n-R)C_{\alpha n}^{i+1}\right],$$

$$F=\frac{1}{(R-1)^3}\left[(R-1)^2C_{\beta\alpha}+2\sum_{n=3,5,\ldots}^{R-2}(n-1)^2C_{\beta n}^{i+1}+4\sum_{n=2,4,\ldots}^{R-1}(n-1)^2C_{\beta n}^{i+1}\right]+R_i^3(C_1-C_0).$$

The value of S_1 at the $(i+1)$th time sequence is determined through the finite difference scheme (16). The calculated S_1 value is utilized to find out the internal node concentration values in β, applying equations (13) and (14). Similarly, S_2 is calculated solving equation (21). Due to the non-availability of concentration values in the α-phase nodes at the $(i+1)$th time sequence, an iteration scheme is adopted as follows. Initially these values are replaced by the ith time sequence values. The estimated value of S_2 (say S_2^*) is substituted in equation (15) to find out the concentration values at the internal nodes of α at the $(i+1)$th time sequence. These values are again substituted in equation (21) to obtain a new estimate of S_2. The process is continued until $|(S_2-S_2^*)/S_2^*|<10^{-6}$.

2.4. $\beta \rightarrow \alpha$ transformation

When the composition of the liquid lies between C_p and $C_{\beta p}$ (Fig. 1), the liquid is consumed earlier than β. The entire amount of liquid is considered to be consumed when S_2 reaches $0.999R_i$. Beyond this point, the transformation proceeds entirely by the growth of α into β. Figure 4 illustrates the finite difference nomenclature applicable to this stage. Concentration inside the β-phase may still be obtained through equations (13) and (14). In the modified configuration of the transformation cell, the diffusion field equation (10) for the α-phase takes the form

$$\frac{dC_n^{\alpha}}{dt} = \frac{\partial C_n}{\partial r_n}\left[\frac{R_i - r_n}{R_i - S_1}\right]\frac{dS_1}{dt} + D_{\alpha}\left[\frac{\partial^2 C_n}{\partial r_n^2} + \frac{2}{r_n}\frac{\partial C_n}{\partial r_n}\right]. \quad (22)$$

The corresponding finite difference representation is as follows:

$$\frac{C_n^{i+1} - C_n^{i}}{\Delta t} = \left(\frac{N-n}{R_i - S_1^i}\right)\left(\frac{C_{n+1}^{i} - C_{n-1}^{i}}{2}\right) \times \left(\frac{S_1^{i+1} - S_1^i}{\Delta t}\right) + D_{\alpha}\left(\frac{N-R}{R_i - S_1^i}\right)^2 \times (C_{n-1}^{i} - 2C_n^{i} + C_{n+1}^{i}) + D_{\alpha} \times \left(\frac{N-R}{R_i - S_1^i}\right)\frac{(C_{n+1}^{i} - C_{n-1}^{i})}{\left[S_1^i + \frac{n-R}{N-R}(R_i - S_1^i)\right]}. \quad (23)$$

Due to the impingement of diffusion fields, concentration at the outer boundary of α at a particular time instant is calculated through $C_{N+1}^{i} = C_{N-1}^{i}$ by considering a virtual $(N+1)$th grid outside the zero mass transfer boundary (cf. Fig. 4). The β–α boundary position is determined through the modified equation

$$\frac{S_1^{i+1} - S_1^i}{\Delta t} = \frac{1}{C_{\beta\alpha} - C_{\alpha\beta}}\left[D_{\alpha}\left(\frac{N-R}{R_i - S_1^i}\right) \times \left(\frac{-C_{R+2}^{i} + 4C_{R+1}^{i} - 3C_{\alpha\beta}}{2}\right) - D_{\beta}\left(\frac{R-1}{S_1^i}\right)\left(\frac{C_{R-2}^{i} - 4C_{R-1}^{i} + 3C_{\beta\alpha}}{2}\right)\right]. \quad (24)$$

The β-phase is assumed to be depleted when S_1 reaches $0.001R_i$. At this point the calculations are terminated.

3. RESULTS AND DISCUSSION

3.1. Comparison with the experimental data

Figures 5 and 6 compare the predictions of the present model with the experimentally determined β dissolution rate from the Cd–5 at.% Ag [33] and Pb–33.3 wt% Bi [34] alloys, respectively. Parametric values used for the calculations are presented in Table 1. For comparison, the results predicted by the models of Maxwell and Hellawell [6], Lopez [21], and Das *et al.* [23] are also incorporated in Figs 5 and 6. In both the systems, the kinetics predicted by the present model have deviated from the experimental data beyond about 65–85% β-dissolution, perhaps, due to the isolation and expulsion of the liquid leading to cavity formation and/or the variation in shape and size of the β-particles in the microstructure, as pointed out in the earlier publications by the authors [23, 24]. It may initially appear from Figs 5 and 6 that the predictions of the Lopez model are in close agreement with the present numerical analysis. However, when the Lopez model assumes a cored profile in β, the predicted results exhibit wide deviation from the experimental kinetics right from the onset of the transformation. As the Pb-rich β-phase in the Pb–Bi system is usually cored, this perhaps, indicates that the quasi-static interface approach of the

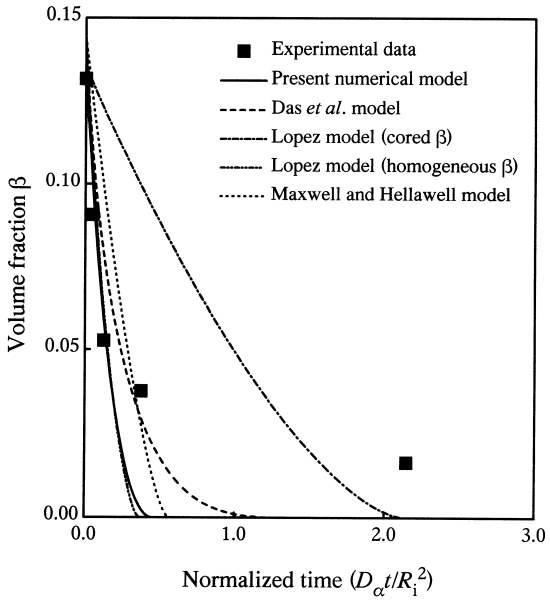

Fig. 5. Volume fraction of the β-phase as a function of normalized time $(D_\alpha t/R_i^2)$ for isothermal peritectic transformation in a Cd–5 at.% Ag alloy at 608 K.

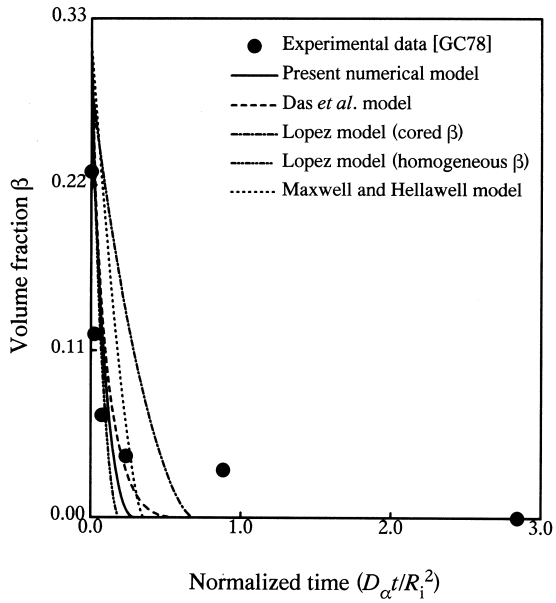

Fig. 6. Kinetics of peritectic transformation in a Pb–33.3 wt% Bi alloy at 443 K.

Table 1. Input parameters used for the calculation of peritectic transformation kinetics in Cd–Ag and Pb–Bi systems by the numerical model

System	C_0 (at. fr. B)	T_1 (K)	R_i (m)	K_1	K_2	Composition (at. fr. B)†				D (m^2/s)
						$C_{\beta\alpha}$	$C_{\alpha\beta}$	$C_{\alpha l}$	C_l	
Cd–Ag‡	0.05	608	1.2×10^{-4}	0.829	2.69	0.193	0.070	0.040	0.016	10^{-12}
Pb–Bi§	0.33	443	1.0×10^{-4}	0.579	2.00	0.216	0.285	0.330	0.443	10^{-14}

†Calculated kinetics were similar for concentration values expressed in volume fraction. ‡The compositions are noted from the equilibrium diagram of the Cd–Ag system [35]. §The compositions are noted from the equilibrium diagram of the Pb–Bi system [35]. R_i was estimated from the size of β-particles in the quenched microstructure prior to peritectic transformation [33, 34] and D estimated from Ref. [36].

Lopez model may not be appropriate for predicting the kinetics. Considerable deviation from experimental results is also observed for the Maxwell–Hellawell model (Fig. 6) apparently because it overlooks the effect of diffusional impingement. The present analysis thus appears to be somewhat better in predicting the kinetics of peritectic transformation as compared to the earlier proposed models of Lopez [21], and Maxwell and Hellawell [6]. Figures 5 and 6 also show that the analytical model of Das *et al.* produces a relatively slower kinetics as compared to that by the more rigorous numerical model. In spite of this, both the models are in remarkable agreement in predicting the kinetic trend of peritectic transformation [33].

3.2. *Effect of concentration profile*

To investigate the effect of coring in the solid phases, transformation kinetics have been calculated for the phase diagrams presented in Fig. 7 at a given temperature, T_1. In the numerical calculations, the diffusivities in both the solids are assumed to be identical and equal to 10^{-11} m^2/s. Other parametric values used in the calculations are reported in Table 2 against the corresponding serial number of the curves. Figure 8 illustrates the effect of α-phase concentration profile on the kinetics of peritectic transformation at T_1 in an alloy of composition $C_0 = 0.35$ in Fig. 7(a). For this alloy, the equilibrium microstructure would consist of (α + liquid) at T_1, so that the peritectic transformation continues until β is entirely consumed. It is assumed that β inherits a cored profile at $t = 0$, while the concentration profile in α is allowed to be cored or linear initially or linear throughout the transformation. The time and distance scales are normalized by the respective multipliers D_α/R_i^2 and $1/R_i$ for an effective comparison between different calculations. Figure 8 reveals that the kinetics predicted for an initially linear or cored composition profile in α are almost identical. Therefore, it is apparent that a cored profile in α may not produce much difference in the rate of the peritectic transformation. In contrast, when α is assumed to retain a linear compositional gradient throughout the transformation, considerable reduction in the rate of both β–α and α–liquid interface migration results, i.e. it underestimates the transformation kinetics. This, perhaps, explains the divergence between the kinetics predicted by the present numerical model and the analytical model of Das *et al.* in Figs 5 and 6 as the latter approximates a linearized gradient in the α-phase throughout the transformation.

Earlier, Lopez [21] proposed that coring in β may result in a significantly slower transformation kinetics, when the volume fraction of β in the microstructure is substantial. Figures 5 and 6 display this trend in the results from the calculation based on the Lopez model. Furthermore, the Lopez model predicted an inexplicable enhancement in the kinetics due to coring when the volume fraction of β in

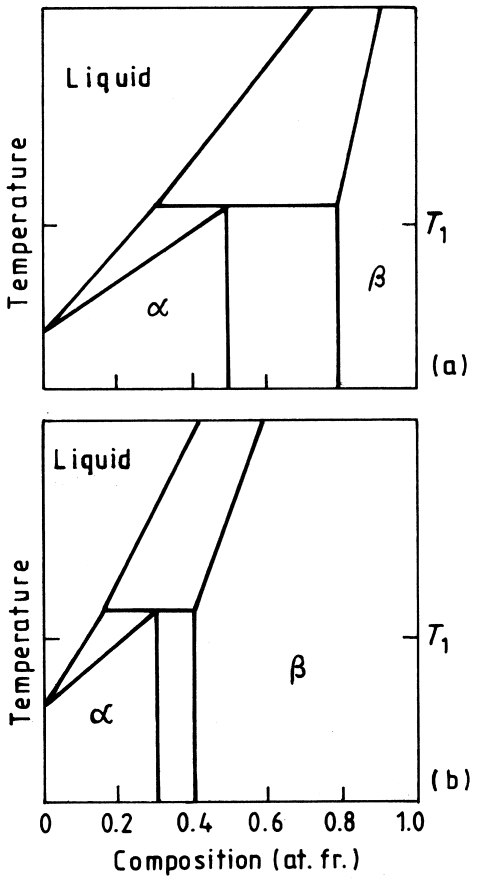

Fig. 7. (a, b) Schematic peritectic phase diagrams utilized to calculate the effect of coring in the solids on the peritectic transformation kinetics.

Table 2. Input variables for the numerical calculations

Run No.	C_0 (at. fr.)	K_1	K_2	Equilibrium compositions (at. fr.)						R_i (m)	D_β (m^2/s)	D_α (m^2/s)
				$C_{\beta p}$	C_{lp}	$C_{\beta\alpha}$	$C_{\alpha\beta}$	$C_{\alpha l}$	C_l			
1	0.35	0.286	1.667	0.80	0.30	0.80	0.50	0.435	0.262	5×10^{-3}	10^{-11}	10^{-11}
2	0.40	0.286	1.667	0.80	0.30	0.80	0.50	0.435	0.262	5×10^{-3}	10^{-11}	10^{-11}
3	0.50	0.286	1.667	0.80	0.30	0.80	0.50	0.435	0.262	5×10^{-3}	10^{-11}	10^{-11}
4	0.23	0.706	2.000	0.40	0.15	0.40	0.30	0.240	0.120	5×10^{-3}	10^{-11}	10^{-11}
5	0.30	0.706	2.000	0.40	0.15	0.40	0.30	0.240	0.120	5×10^{-3}	10^{-11}	10^{-11}

the microstructure was smaller. To estimate the effect of concentration gradient in β, calculations were performed through the present numerical model for compositions $C_0 = 0.4$ and 0.5 corresponding to the phase diagram in Fig. 7(a) at T_1. The former alloy composition allows estimation of the effect of β-coring on the kinetics of peritectic transformation and, the latter on the kinetics of β–α transformation following an early liquid consumption. The results are presented in Figures 9 and 10. In all the calculations, initially a cored composition profile has been assigned to α, while β is assumed to be initially cored or homogeneous. Contrary to the predictions of Lopez, Figs 9 and 10 demonstrate that coring in β has almost no effect on the kinetics of the α–liquid interface migration. On the other hand, the effect of the same on the β–α interface movement is negligible during the peritectic transformation (Fig. 9). After the consumption of the liquid, coring produces a marginal retardation of this interface migration kinetics (Fig. 10). It may be noted that in Fig. 10 (and in the subsequent figures) the liquid consumption is complete when the α–liquid interface position reaches the value 1.0 in the normalized interface position scale. Figures 11 and 12 present similar plots for the phase diagram in Fig. 7(b) for the compositions $C_0 = 0.23$ and 0.3, respectively, at T_1. In this case, coring produces a steeper concentration gradient in β, and consequently, its effect on the kinetics should be relatively more pronounced. Here, a cored profile in β produces a slower kinetics from the beginning of the transformation, although the effect is relatively more pronounced after the consumption of the liquid (cf. Fig. 11 with Fig. 12). Nevertheless, the effect of β-coring on the peritectic transformation kinetics is not as significant as that described earlier [21]. It may be pointed out that in addition to the pre-existing concentration gradient in β, D_β also determines the solute flux from β to α. However, calculations through the present model indicate that a change in D_β produces a negligible change in the kinetics [33].

In summary, the present investigation shows that contrary to the earlier predictions [21], no significant deviation in kinetics arises out of coring in β (Figs 9–12). Moreover, the effect of β-coring on the kinetics is relatively more pronounced for alloy compositions where the liquid is consumed earlier during the transformation (Figs 10 and 12) as diffu-

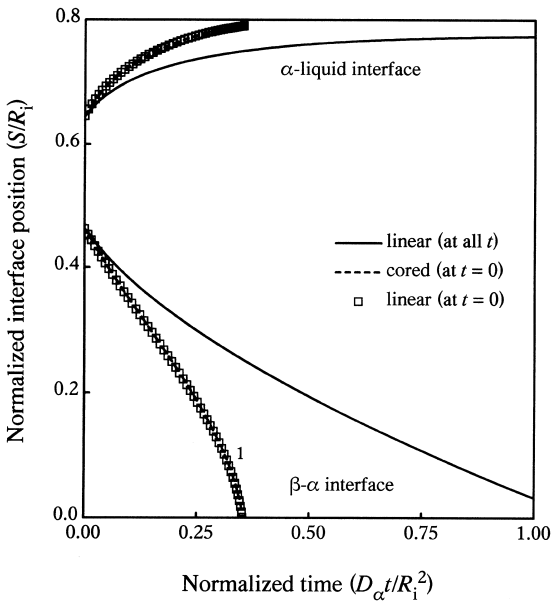

Fig. 8. Effect of concentration profile in α on the kinetics of the peritectic transformation shown in Fig. 7(a) at T_1.

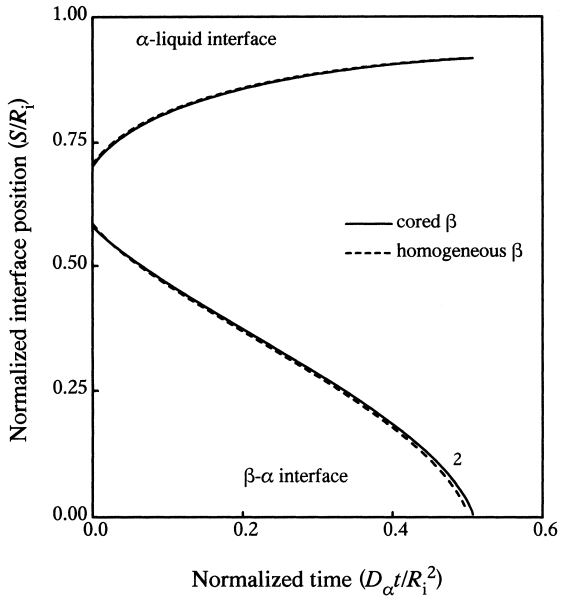

Fig. 9. Influence of concentration profile in β on the kinetics of peritectic transformation illustrated in Fig. 7(a) for an alloy composition $C_0 = 0.45$ at T_1.

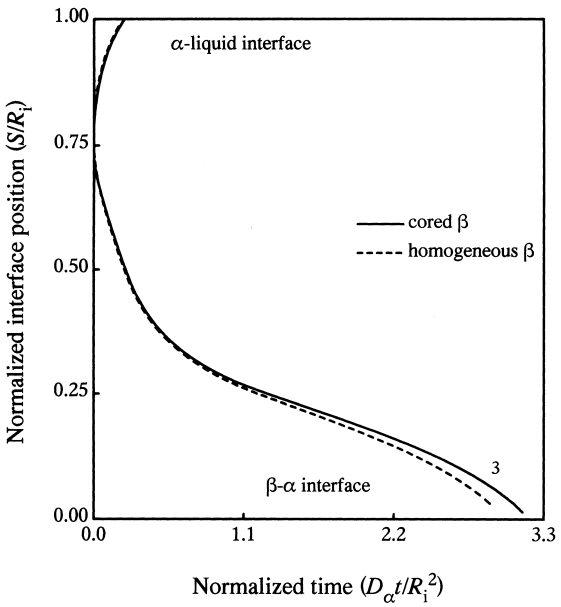

Fig. 10. Kinetics of peritectic and β–α transformation following liquid consumption in the presence of cored or homogeneous β-phase for an alloy of peritectic composition in Fig. 7(a) at T_1.

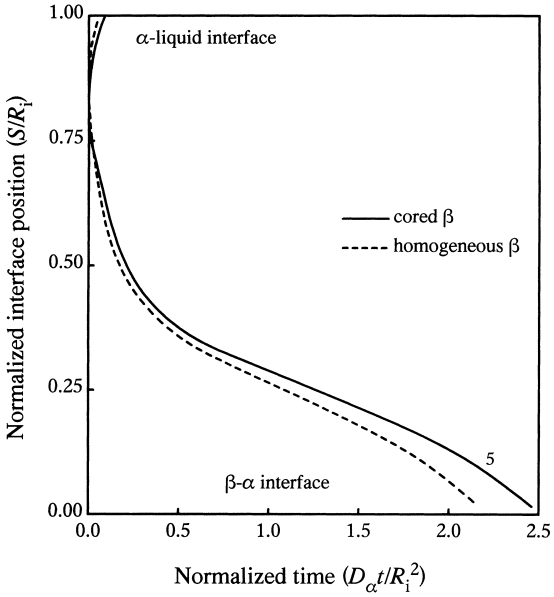

Fig. 12. Influence of solute segregation in β on the kinetics of peritectic and β–α transformation following liquid consumption for an alloy of peritectic composition in Fig. 7(b) at T_1.

sional impingement brings down the concentration gradient in the α layer. Therefore, it appears that the concentration profile in β affects the peritectic transformation kinetics only when it can dominate over the effect of concentration gradient existing at the α-side of the β–α boundary. Consequently, a more restricted compositional field in α is expected to enhance the effect of coring in β and calculations through the present numerical model have shown a similar trend [33]. Thus, the composition range in α determines the effect of β-coring on the peritectic transformation kinetics in contrast to the volume fraction of β in the microstructure as predicted earlier by Lopez [21]. It appears that the approximations of quasi-static interface and time-invariant concentration profile as in the Lopez analysis may not be always realistic for the calculation of the peritectic transformation kinetics.

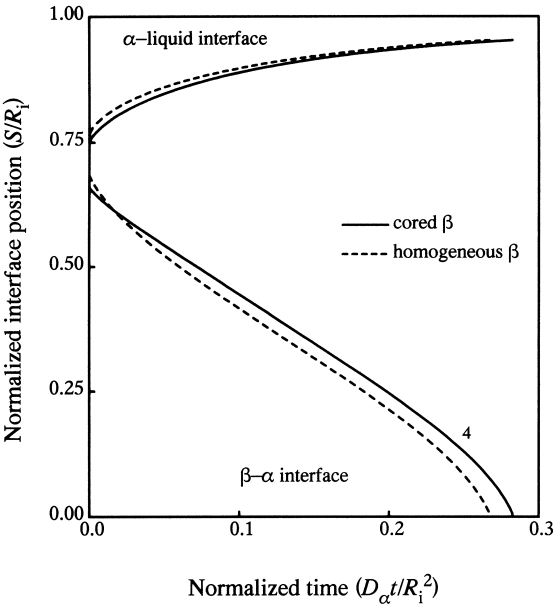

Fig. 11. Effect of coring in β on the kinetics of peritectic transformation for an alloy of composition $C_0 = 0.23$ in Fig. 7(b) at T_1.

4. CONCLUSIONS

1. A rigorous numerical model on the kinetics of peritectic transformation has been presented that is capable of considering unsteady state diffusion in finite moving phase fields. Predictions from the present model show a better agreement with the experimental kinetic data from the Cd–Ag and Pb–Bi systems, when compared to those obtained from the existing theoretical formulations based on quasi-static interface position, time-invariant concentration profile, and Laplacian profile approximations.
2. The calculated kinetics deviate from the experimental one approximately beyond 65–85% of β-dissolution, possibly due to the latter deviating from the idealized configuration of the transformation cell considered in the theoretical calculations.
3. Both cored and linear initial concentration profiles in α appear to have a similar effect on the transformation kinetics. However, the kinetics

may be underestimated if the concentration gradient in α is assumed to be linear throughout the transformation.

4. Coring in the β-phase has no appreciable effect on the migration of the α–liquid interface. On the other hand, the effect of the same on the β–α interface movement is marginal and assumes significance only after the consumption of the liquid and in the presence of a shallower composition gradient in α.

REFERENCES

1. Pelton, A. D., in *Thermodynamics and Phase Diagrams in Materials, Materials Science and Technology*, Vol. 5, ed. R. W. Cahn, P. Haasen and E. J. Kramer. VCH Verlagsgesellschaft GmbH, Weinheim, 1991, p. 33.
2. Kerr, H. W. and Kurz, W., *Int. Mater. Rev.*, 1996, **41**, 129.
3. Chuang, Y. K., Reinisch, D. and Schwerdtfeger, K., *Metall. Trans.*, 1975, **61A**, 235.
4. Crosley, F. A. and Mondolfo, L. F., *Trans. metall. Soc. A.I.M.E.*, 1951, **191**, 1143.
5. Maxwell, I. and Hellawell, A., *Trans. metall. Soc. A.I.M.E.*, 1972, **3**, 1487.
6. Maxwell, I. and Hellawell, A., *Acta metall.*, 1975, **23**, 901.
7. VanWiggen, P. C. and Alsem, W. H. M., in *Light Metals, Proc. TMS Annual Meeting*, Warrendale, Pennsylvania, 1993, p. 763.
8. Sawano, K., Morita, M., Miyamoto, K., Doi, K., Hayashi, A. and Murakami, M., *J. Ceram. Soc. Japan*, 1989, **97**, 1028.
9. Goyal, A., Funkenbusch, P. D., Kroger, D. M. and Burns, S. J., *Physica C: Superconductivity*, 1991, **182**, 203.
10. Jee, Y. A., Kang, S. J. L., Suh, J. H. and Yoon, D. Y., *J. Am. Ceram. Soc.*, 1993, **76**, 2701.
11. Pellerin, N., Odier, P., Simon, P. and Chateigner, D., *Physica C: Superconductivity*, 1994, **228**, 351.
12. Kim, C. J., Kim, K. B. and Hong, G. W., *Mater. Lett.*, 1994, **21**, 9.
13. Ullrich, M. and Freyhardt, H. C., *Physica C: Superconductivity*, 1994, **235-240**, 455.
14. Kajitani, T., Nagayama, K. and Umeda, T., *J. Magn. Magn. Mater.*, 1992, **117**, 379.
15. Kwon, H. W., Bowen, P. and Harris, I. R., *J. Alloys Compounds*, 1992, **189**, 131.
16. Chen, Z., Wang, N., Song, X. and Wang, X., *Acta metall. sin.*, 1994, **7**, 95.
17. Chen, Z., Wang, N., Song, X. and Wang, X., *Mater. Lett.*, 1995, **22**, 119.
18. Titchner, A. P. and Spittle, J. A., *Metals Sci.*, 1974, **8**, 112.
19. St. John, D. H. and Hogan, L. M., *Acta metall.*, 1977, **25**, 77.
20. Wagner, C., *Acta metall.*, 1969, **17**, 99.
21. Lopez, H. F., *Acta metall. mater.*, 1991, **39**, 1543.
22. Pabi, S. K., *Acta metall.*, 1979, **27**, 1693.
23. Das, A., Manna, I. and Pabi, S. K., *Scripta mater.*, 1997, **36**, 867.
24. Das, A., Manna, I. and Pabi, S. K., *Trans. Indian Inst. Met.*, 1998, **51,** 165.
25. Zener, C., *J. appl. Phys.*, 1947, **20**, 962.
26. Fredriksson, H., *Metals Sci.*, 1976, **10**, 77.
27. Fredriksson, H. and Nylén, T., *Metals Sci.*, 1982, **16**, 283.
28. St. John, D. H., *Acta metall.*, 1990, **38**, 631.
29. Tanzilli, R. A. and Heckel, R. W., *Trans. Am. Inst. Min. Engrs*, 1968, **242**, 2313.
30. Murray, D. and Landis, F., *Trans. Am. Soc. Min. Engrs*, 1959, **81D**, 106.
31. Crank, J., in *Mathematics of Diffusion.* Oxford University Press, London, 1956, p. 197.
32. Press, H. W., Teukolsky, S. A., Vetterling, W. T. and Flannery, B. P., in *Numerical Recipes in Fortran.* Cambridge University Press, Cambridge, 1992, p. 127.
33. Das, A., Ph.D. thesis, I.I.T. Kharagpur, India, 1997.
34. Goddard, D. M. and Childs, W. J., *J. less-common Metals*, 1978, **58**, 217.
35. Massalski, T. B. (ed.), *Binary Alloy Phase Diagrams*, Vol. 1. ASM International, Materials Park, Ohio, 1990.
36. Smithels, C. J. and Brandes, E. A. (ed.), *Metals Reference Book*. Butterworth, London, 1976, p. 877.